In Robotics and Automation Magazine, 1(2), pp. 4-13, June 1994.

Analysis and Experimental Verification of a Fourth Order Plant Model for Manipulator Force Control

Richard Volpe * and **Pradeep Khosla** †

Abstract

This paper presents the analysis and experimental verification of a fourth order model of the arm / sensor / environment system plant, to be use in evaluation of force control strategies. Both the undamped and underdamped cases are investigated. Approximations and qualifications, based on the reality of our experimental system, help reduce the solution to just a few dominant terms. Comparing these terms with experimental data of the system undergoing small oscillations yields approximate values for all of the parameters in the model. To justify the obtained values, and thereby the approximations used, two measures are taken. First, a simulation of the fourth order model is performed, and compared against experimental data obtained from the CMU DD Arm II system. Second, a stability analysis of several force control schemes acting on the modelled plant is reviewed and compared against experimental tests of the controllers. In both cases, the simulation and analysis match closely with the experimental results, confirming the validity of the plant model.

1 Introduction

There exist a large number of capabilities needed for automation which require control of the forces of interaction between a robot and its environment. Examples include pushing, pulling, scraping, grinding, twisting, etc. While performing these tasks, the system may be considered to consist of two components: the force feedback controller and the arm / sensor / environment plant. Many types of algorithms have been proposed for force control of robots [15]. However, analysis of them is often based on an assumed plant model, with parameter values that are not experimentally derived [4, 2, 1]. Alternatively, some researchers have experimentally developed a compensator that works for their plant [16, 5, 6]. But this approach often yields little understanding into the physics of the of the plant, preventing analysis of alternative compensators. The obvious merger of these two solution techniques requires the experimental extraction of a physical model, and the design and analysis of compensators by using the model. This paper describes in detail the first part of this solution: experimental extraction of physical system model parameters. Elsewhere, we have used the parameters in the model to analyze the wide variety of force control strategies, and confirmed the analysis and model with experimental implementation of the strategies [11, 12].

*Currently at The Jet Propulsion Laboratory (MS 198-219), California Institute of Technology, Pasadena, California 91109. (Email: volpe@telerobotics.jpl.nasa.gov) This work was completed while the author was a member of the Department of Physics, The Robotics Institute, Carnegie Mellon University, Pittsburgh, Pennsylvania, 15213.

†Department of Electrical and Computer Engineering, The Robotics Institute, Carnegie Mellon University, Pittsburgh, Pennsylvania, 15213. (Email: pkk@ece.cmu.edu)

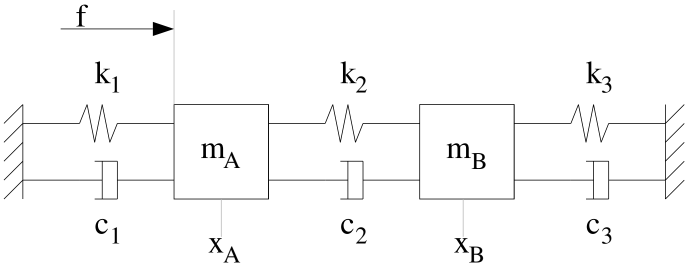

Figure 1: General fourth order model of the arm, sensor, and environment system.

In order to have a basis for the experimentation presented herein, a fourth order plant model has been hypothesized, based on an assumption that the first mode of vibration is dominant in the system components [9, 3]. This model is shown in Figure 1, where f is the actuation force; x_A is the measured position of the arm; x_B is the position of the environment; and m, k, and c are the mass, stiffness, and damping parameters. This is similar to the model presented in [4]. However, the following analysis will result in different parameter values for the system, and leads to different predicted behavior for the force controllers having this system as a plant [11].

This paper is organized as follows: Section 2 outlines a vibration analysis of the model for the undamped and underdamped, low frequency oscillation cases. Also presented is an approximate relation between the measured force and the position and velocity of the first oscillatory mass. Section 3 reviews the formulation of force versus position/velocity ellipses representing damped oscillations. Then Section 4 presents the methods and results for static and low frequency oscillation experiments. Step by step, it is shown how all system parameters are extracted, either directly or through judicious approximations. Section 5 presents the results of using the extracted parameters in a simulation of the fourth order system, showing favorable comparison with the experimental data. Finally, Section 6 reviews the results of utilizing the derived model as a plant in explicit force control schemes. It is shown that this analysis correctly predicts the experimentally measured response of the system under several force control strategies. The correct predictions further confirm the validity of the model, and the extracted parameters.

2 Vibrational Analysis

This section provides a vibration analysis of the model shown in Figure 1. Similar analysis can be found in many standard physics textbooks [7]. However, the analysis here deals with the asymmetric case and an approximate result will be presented for the case of underdamped vibration.

Using the general solution of $x = Ce^{\pm pt}$ the equations of motion for the model may be written as:

$$\begin{bmatrix} m_A p^2 + c_A p + k_A & -(c_2 p + k_2) \\ -(c_2 p + k_2) & m_B p^2 + c_B p + k_B \end{bmatrix} \begin{bmatrix} x_A \\ x_B \end{bmatrix} = \begin{bmatrix} f \\ 0 \end{bmatrix} \tag{1}$$

where p is a complex number ($p = \sigma \pm i\omega$) and

$$k_A = k_1 + k_2 \qquad c_A = c_1 + c_2 \tag{2}$$
$$k_B = k_2 + k_3 \qquad c_B = c_2 + c_3. \tag{3}$$

The characteristic equation may be obtained from Equation (1) with $f = 0$:

$$\begin{aligned} p^4 m_A m_B + p^3(m_B c_A + m_A c_B) \; + \; & p^2(m_B k_A + m_A k_B + c_A c_B - c_2^2) \\ & + \; p(c_B k_A + c_A k_B - 2c_2 k_2) + (k_A k_B - k_2^2) \; = \; 0 \end{aligned} \tag{4}$$

For our experiments with the CMU DD Arm II , $k_1 = 0$ since the manipulator has no gearing, and no position dependent term is used in the controller during model identification. It is also assumed the $k_2 \gg k_3$, since k_2 is provided by the aluminum link and sensor stiffness, whereas k_3 represents a softer environment composed of a cardboard box with an aluminum plate resting on it. Using these assumptions about the stiffness parameters, the eigenvalues for this system in the undamped case ($c_1 = c_2 = c_3 = 0$) are:

$$\omega_l \approx \sqrt{\frac{k_3}{m_A + m_B}} \qquad \text{and} \qquad \omega_h \approx \sqrt{k_2\left(\frac{1}{m_A} + \frac{1}{m_B}\right)} \quad . \tag{5}$$

These results make intuitive sense. The lower frequency ω_l corresponds to the case of m_A and m_B acting as a rigid body oscillating on k_3. Similarly, the higher frequency ω_h corresponds to the case of m_A and m_B oscillating out of phase on spring k_2, neglecting any effect of k_3.

In the damped system, solving for p will yield two complex solutions and their conjugates. For the underdamped case, the poles will be close to the undamped poles, but moved slightly to the left of the imaginary axis. Considering the case of the low frequency oscillation, m_A and m_B oscillate in phase on k_3, with damping from only c_1 and c_3. This is essentially a second order system with poles:

$$p = \frac{c_1 + c_3}{2(m_A + m_B)} \pm \sqrt{\frac{(c_1 + c_3)^2}{4(m_A + m_B)^2} - \frac{k_3}{(m_A + m_B)}} \tag{6}$$

indicating that the decay parameter is

$$\sigma = \frac{c_1 + c_3}{2(m_A + m_B)}. \tag{7}$$

This estimation will prove useful later in the paper when analyzing data of the oscillations of the real system.

This low frequency approximation, however, precludes the measurement of force, which depends on the compression of spring k_2:

$$f_m = k_s \Delta x_s = k_2(x_B - x_A). \tag{8}$$

where s indicates the sensor stiffness and compression. A further complication is the fact that it is not possible to directly measure the value of x_B (at least with our experimental system).

One possibility for determining an analytic expression for f_m is to solve Equation (4) for p exactly, and substitute these solutions into Equation (1) to obtain the relation between x_A and x_B. However, this brute force method would provide an algebraically complicated solution, yielding little intuitive insight. Instead, we have previously shown [9, 10] that the transfer functions for x_A/x_B given in Equations (1) can be used in Equation (8) to obtain an approximation of the measured force in terms of only x_A (and its derivative):

$$\begin{aligned} f_m \;\; &\approx \;\; -\frac{k_3}{\alpha} x_A + \left[c_1 - c_3 + c_2 \frac{k_3}{k_2 \alpha}\right] \dot{x}_A && (9) \\ &= \;\; -K' x_A - C' \dot{x}_A && (10) \end{aligned}$$

where K' and C' are the effective stiffness and damping, and α is the ratio $(m_A + m_B)/m_A$ [10].

The relationship of f_m to x_A seems reasonable — the measured force is equal to the value of $-k_3 x_A$, modified only be the parameter α. But the value of C' seems strange at first glance. Obviously, the introduction of damping to the system can make the measured force proportional to the velocity, $\dot{x}_A$. However, it can be seen that this term may take on negative and positive values. For positive values, it appears at first that the system is not conservative. But a very simple and intuitive explanation can be provided to show that the system remains a conservative one.

When the system is oscillating at the low eigenfrequency the masses are moving symmetrically, with m_A having a slightly larger amplitude than m_B [10]. As m_A moves toward the environment, k_2 is compressed and a force is measured. However, the dampers c_1 and c_2 resist the motion of m_A. Thus, they both diminish the magnitude of the measured force. This is in contrast to the force caused by c_3 which resists the motion of m_B away from m_A, increasing the measured force.

In summary, the introduction of damping to the oscillatory system has caused a change of phase of the oscillations. This phase change shows up as a velocity term in our approximation for the measured force. In the next section the effects of this phase change on the system will be detailed.

3 Damped Oscillations

When damping is added to an oscillating system, energy is lost during the cycle of motion. If the oscillation is maintained by a driving force, then the energy lost due to damping is replaced every cycle. However, the addition and subtraction of energy are not in phase. If they were, the damping would be instantaneously negated, and the system would oscillate as if it were undamped.

Consider the fourth order system that we have been analyzing. Equation (10) shows that this may be thought of as a second order system with an arbitrary mass on spring and damper, K' and C'. In this reduced model, the measured force f_m is equivalent to the sum of the forces experienced by the mass:

$$f = m\ddot{x} = -K'x - C'\dot{x} \tag{11}$$

(For convenience, the subscripts have been dropped.) For such a system, the quasi-static motion of x would yield a straight line of slope $-K'$ and maximum x deviations of A, as shown in Figure 2. (Note, this figure contains an offset $f_0 = -K'x_0$ which may be added to both sides of the above equation.) For the dynamic situation in which the damped system is driven so that there is no loss in amplitude, the force is described by Figure 3. It is no longer a straight line but a loop. This makes intuitive sense. Since the value of f is no longer dependent on just x, but also on the direction of motion. Motion in the positive direction causes the measured force to be reduced by a negative damping force. Motion in the negative direction causes the measured force to be increased by a positive damping force.

It has been shown that this loop is an ellipse for steady state oscillations [8, 10]:

$$\left(\frac{F_D}{C'A\omega}\right)^2 + \left(\frac{x}{A}\right)^2 = 1 \tag{12}$$

To obtain the direction of travel about this curve note that when passing through x_0 and moving in the negative x direction, the damping force, $-C'\dot{x}$, must be positive for $C' > 0$. Thus, for $C' > 0$, the direction of travel around the loop is counterclockwise. For $C' < 0$, it is clockwise.

However, this is just the description of the damping force. To get the value of the measured force we must add the spring force as in Equation (11). This is the equivalent of adding a line to an ellipse. The addition of a line to an ellipse mathematically yields a rotated ellipse, but the

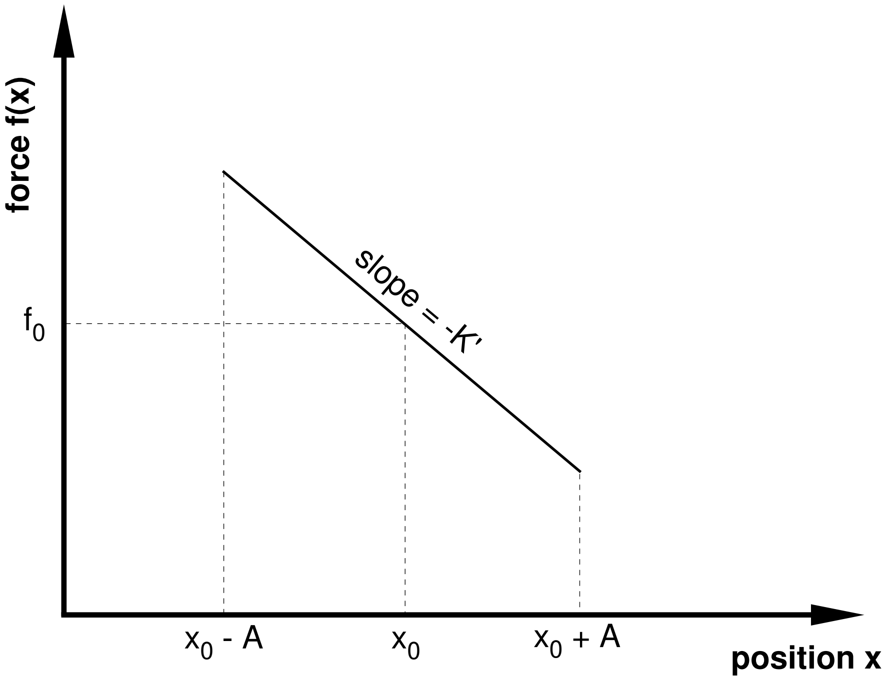

Figure 2: Linear relationship of force to displacement.

semi-major axis is not parallel to the line. Since the slope of the line added is important, we will think of the new contour as a *skew ellipse*. Thus, the addition of the spring force to the damping force yields the measured force as a skew ellipse with an axis at slope $-K'$, as shown in Figure 3.

A similar analysis may be performed for the curve of $f(\dot{x})$ which again yields an ellipse. The direction of travel about this loop may be obtained by considering the situation at the extremes of oscillation when the velocity is zero. When switching from a positive to negative velocity, the force must be in the negative direction. Thus the direction of travel is clockwise for $K' > 0$.

Again, it is necessary to add an offset to obtain the measured force. From Equation (11) we see that we must add the damping force. This again yields a skew ellipse with an axis at slope $-C'$, as shown in Figure 4.

Finally, if the system is not driven to maintain a constant amplitude the oscillations will decay. This causes the continuous elliptical curves to change to elliptical spirals that converge on the ellipse centers.

4 Experimental Data

To test the model presented, we have obtained experimental data of the arm and environment system under small oscillations. The experimental setup is shown in Figure 5. The environment is a cardboard box with an aluminum plate resting on it. The box is resting on a table that is considerably stiffer than the box, and is therefore considered ground for these tests. The force sensor is mounted on link six of the CMU DD Arm II . Attached to the force sensor is a steel probe with a brass weight on its end. The brass weight serves as an end effector substitute and provides a flat, stiff surface for applying forces on the environment.

The first test was to determine the stiffness of the environment. This was done by quasi-statically depressing the box with the CMU DD Arm II . The resultant force versus position diagram is shown

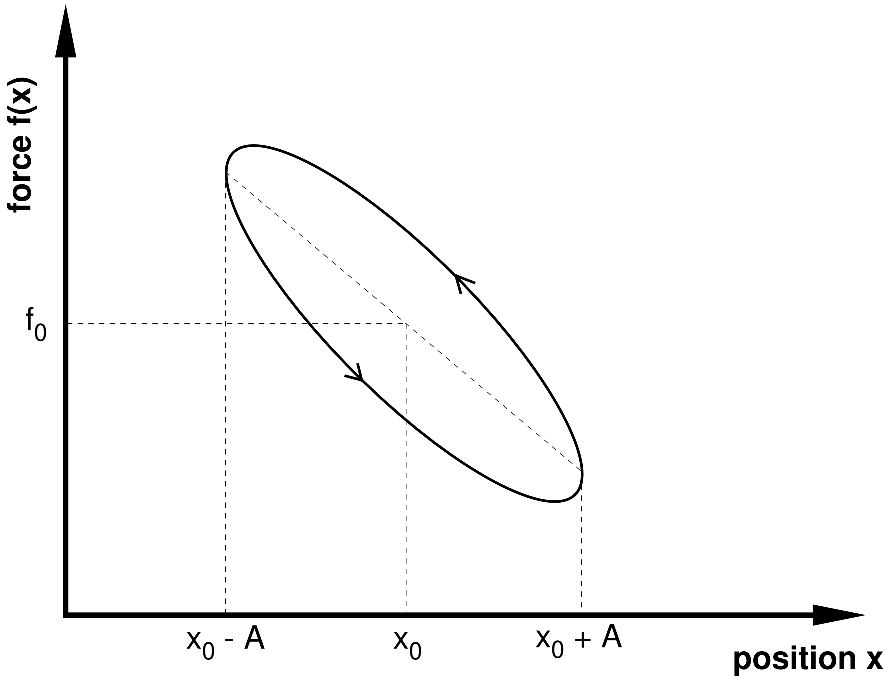

Figure 3: Force as a function of displacement with damping present.

in Figure 6. The graph is linear with a slope of 9340 N/m. This slope is equal to the sequential combination of of k_2 and k_3. However, since k_2 is much larger, the measured spring constant can be reduced to $k_{meas} \approx k_3 \approx 10^4$ N/m.

(Note: In this and all subsequent data charts presented, the parameter f_m may be represented by MezForc_wd[2], the z component of the measured force in the world frame. Similarly, the parameter x_A may be represented by MezP[2], the z component of the measured position in world frame. Also $\dot{x}_A$ is represented by MezXVel_wd[2], the z component of the measured Cartesian velocity in world frame.)

Another test was performed to measure the stiffness of the force sensor. To do this, the sensor was removed from the arm and compressed in a C-clamp. Compression of the sensor was measured with a micrometer, and the forces were measured by the sensor itself. The data is shown in Figure 7. The measured spring constant, k_s, was about 5×10^6 N/m.

We have previously described how k_2 is less than k_s by a geometric proportion factor due to the concatenation of the aluminum sensor with the aluminum arm [10]. For the CMU DD Arm II this factor is on the order of ten. Thus k_2 will be about an order of magnitude less than the force sensor stiffness of 5×10^6 N/m. We also have also assumed in Section 2 that $k_2 \gg k_3$, and therefore k_2 is at least an order of magnitude larger than the environmental stiffness of 10^4 N/m. This implies, $k_3 \ll k_2 \ll k_s$ or 10^4N/m $< k_2 < 5 \times 10^6$N/m. We let $k_2 \approx 5 \times 10^5$.

Given this initial data, and the model development of the previous sections, it is possible to analyze the response of the entire system to small oscillations. To obtain the data, the arm was placed against the environment as shown in Figure 5. The arm was given an open-loop command to exert 20 N of force against the surface. (Incidentally, the measured open-loop force of 18.6 N indicates the need for closed-loop force control.)

A damping gain of $c_1 = 10\,\mathrm{N \cdot s/m}$ was also employed. This value of damping was chosen since it provided reasonable damping during position controlled motion without surface contact. During

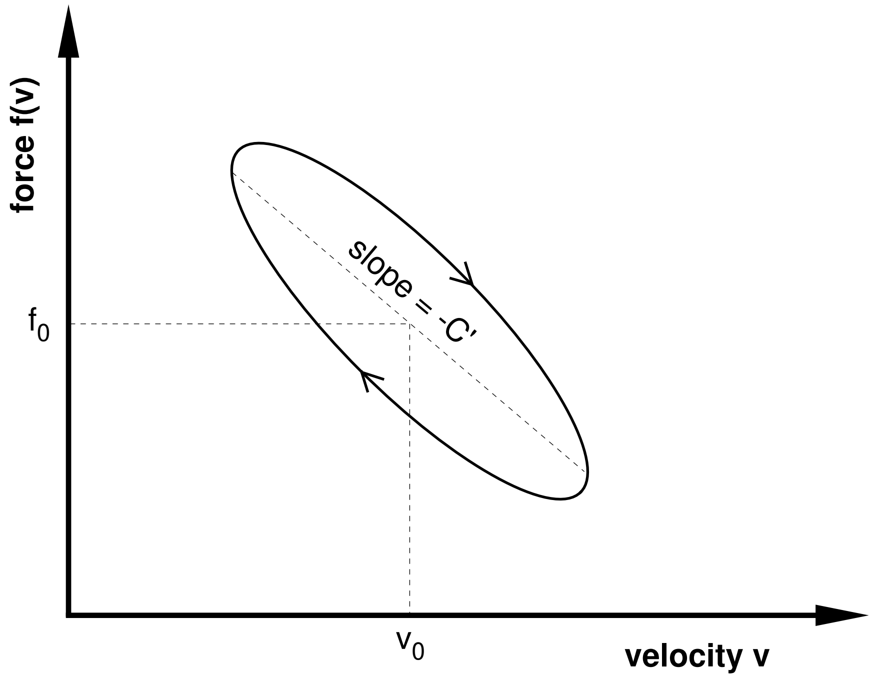

Figure 4: Force as a function of velocity with damping present in the oscillating fourth order system.

contact, the stiffness of the environment makes this gain too small for critical damping. However, it could not be increased for several reasons directly effecting system stability: sampling rate, sensor noise, and plant model consistencies [14].

To measure the system response, the environmental surface was struck softly so as to excite only low frequency oscillations. The measured force, position and velocity of one of these tests is shown as a function of time in Figure 8. While damping is present, the system is obviously underdamped, which matches our earlier assumptions.

First, the frequency of oscillation in Figure 8 is about 90 radians/second. Since only the low frequency mode of oscillation has been excited, ω_l in Equations (5) gives $m_A + m_B = 1.2$ kg.

Second, the environmental damping parameter c_3 may be obtained using Equation (7). Figure 9 is a plot of the natural logarithm of the absolute value of the peak oscillations of the measured force. The slope of the line in this graph gives the value of the decay parameter $\sigma = -11.3$. Thus, $c_3 = -2(m_A + m_B)\sigma - c_1 = 17\ \mathrm{N \cdot s/m}$.

The above time response of force, position, and velocity, may also be graphed to show the damped response. Figure 10 shows the measured force as a function of displacement. The slope of the elliptical spiral yields $K' \approx 10^4$ N/m. Figure 11 shows the measured force as a function of velocity. The slope of this elliptical spiral indicates that $C' \approx 66\,\mathrm{N \cdot s/m}$, which is greater than zero, as explained previously. Figure 12 shows that these are valid values of K' and C' by comparing the measured force with the force calculated from Equation (10). These values of K' and C' may be used in a comparison of Equations (10) and (9) to provide estimates of the remaining model parameters: m_A, m_B, and c_2.

First, we know that $K' \approx k_3/\alpha$. Since both K' and k_3 are approximately 10^4 N/m, $\alpha \approx 1$. However, α cannot be exactly unity or m_B is zero. Therefore, we infer the data indicates that $m_A \gg m_B$. We will assume that $\alpha \approx 1.1$, or equivalently, m_B is less than m_A by an order of

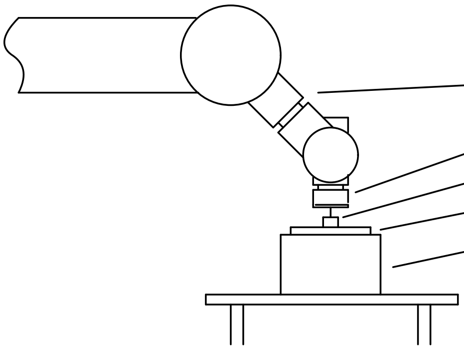

Figure 5: Experimental setup for force oscillation experiments.

magnitude: $m_B = 0.1m_A$. Therefore, from our previous result that $m_A + m_B = 1.2$kg, we have $m_A \approx 1.1$kg and $m_B \approx 0.1$kg.

Second, we know that from Equations (10) and (9) that $c_2 \approx (\alpha k_2/k_3)(C' - c1 + c3) = 4400\,\mathrm{N} \cdot \mathrm{s/m}$.

In review, the following parameters values were obtained using the described means and assumptions:

$k_1 = 0$ N/m	Direct Drive motors have no intrinsic stiffness, and none was provided actively.
$k_3 \approx 10^4$ N/m	Quasi-static measurement of force versus displacement assuming $k_2 \gg k_3$.
$k_s = 5 \times 10^6$ N/m	Direct measurement with the force sensor and a micrometer.
$k_2 \approx 5 \times 10^5$ N/m	Condition that $k_3 \ll k_2 \approx (10^{-1})k_s$.
$m_A + m_B = 1.2$ kg	Measurement of oscillating frequency, assuming low frequency underdamped vibration.
$c_1 = 10\,\mathrm{N} \cdot \mathrm{s/m}$	Controlled damping.
$c_3 = 17\,\mathrm{N} \cdot \mathrm{s/m}$	Measured from decay envelope.
$K' \approx 10^4$ N/m	Measurement of force versus position loop skew.
$C' \approx 66\,\mathrm{N} \cdot \mathrm{s/m}$	Measurement of force versus velocity loop skew.
$m_A = 1.1$ kg, $m_B = 0.1$ kg	$K' \approx k_3$ indicates $\alpha \to 1$. Assume $\alpha \approx 1.1$ or $m_A/m_B \approx 10$.
$c_2 = 4235\,\mathrm{N} \cdot \mathrm{s/m}$	From calculation based on small damping approximation.

In the case of different arm configurations, the only parameter to change would be m_A, due to the change in the arm inertia [11]. From Equations (5), (7), and (10) it is apparent that a change in m_A causes a change in the frequency of oscillation of the system, and rate of decay of these oscillations. This change might manifest itself as a change in the parameters K' and C', and in the slopes of the corresponding ellipses. However, if singular configurations of the manipulator are

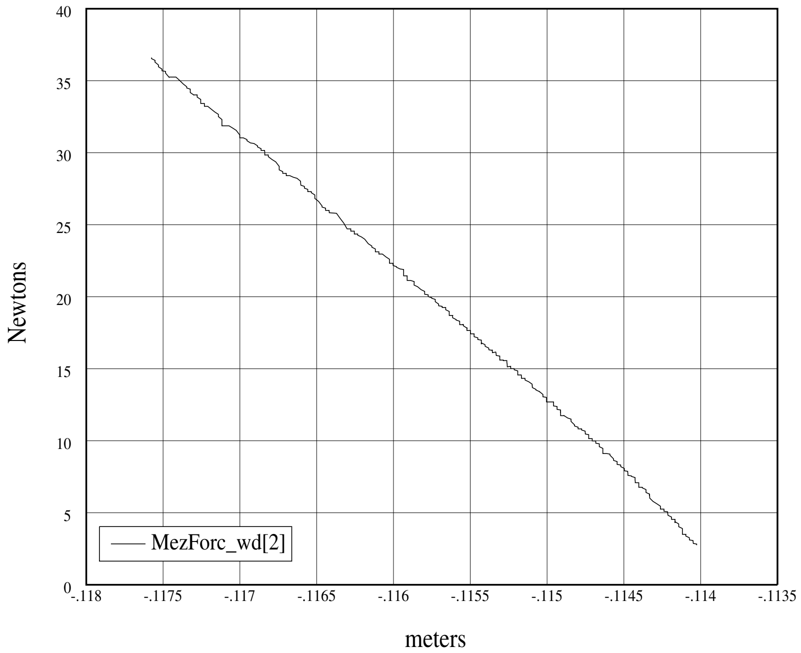

Figure 6: Force versus position data for arm pushing quasi-statically on environment. The slope is approximately $k_e = 9340$ N/m.

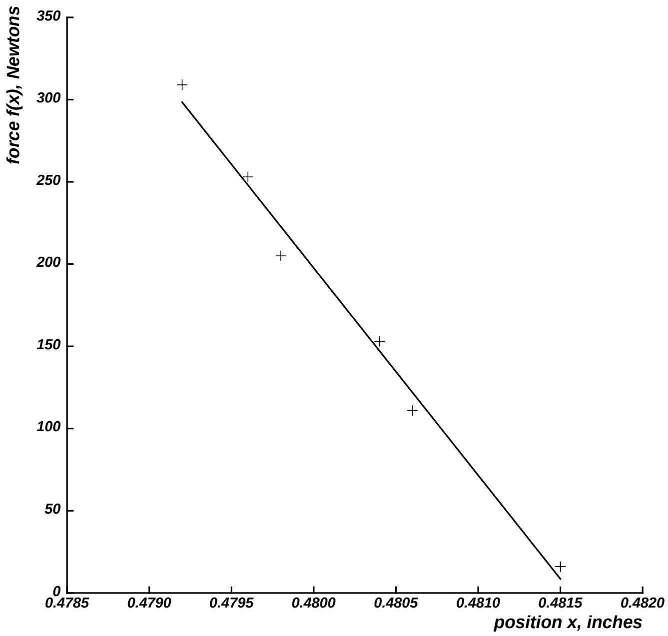

Figure 7: Force versus position data for static compression of force sensor with a clamp. The slope is $k_s = 5 \times 10^6$ N/m.

.

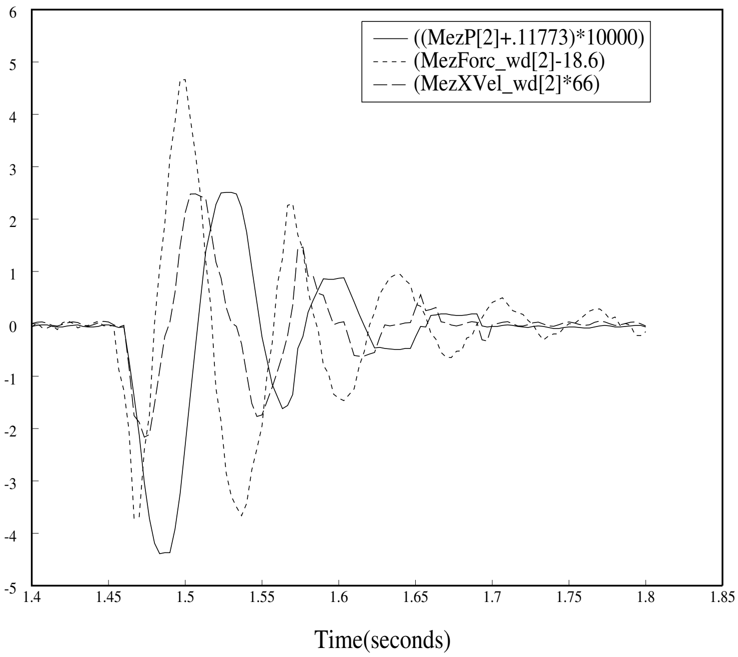

Figure 8: The measured time response of force, position, and velocity after the system has been excited.

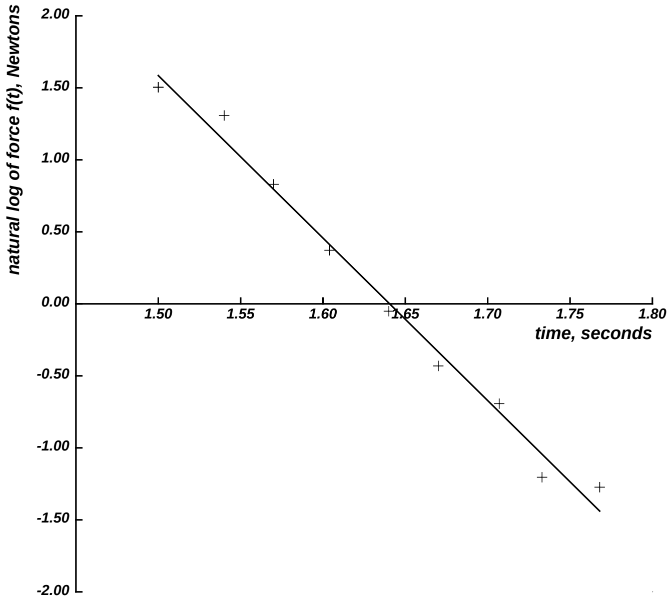

Figure 9: The measured damping of the environment. The slope of -11.3 is the decay constant of the environment.

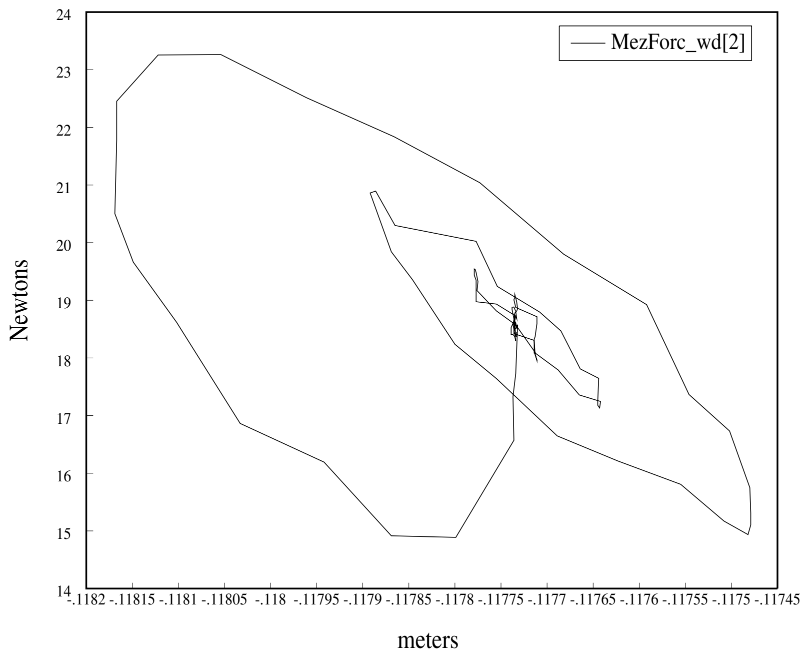

Figure 10: The measured response of force versus position for the fourth order system with damping present.

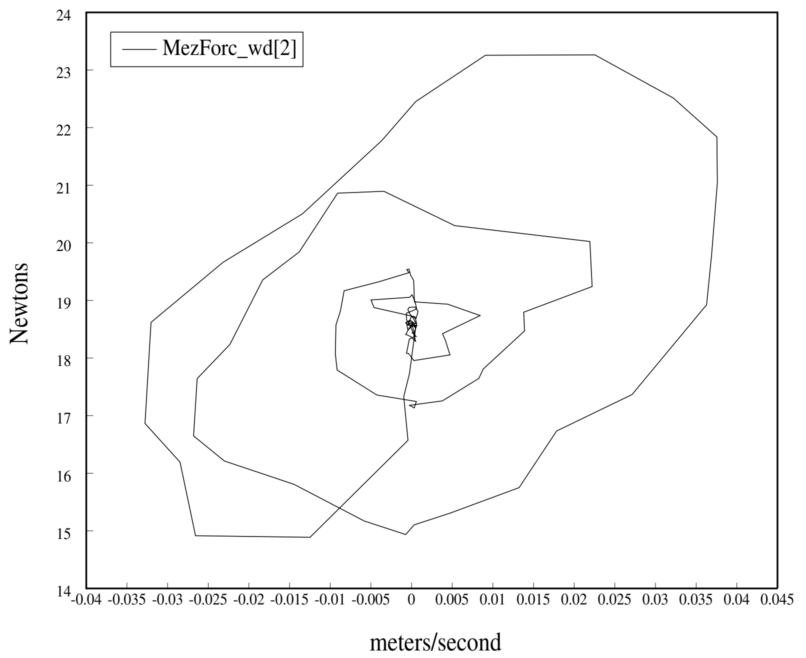

Figure 11: The measured response of force versus velocity for the fourth order system with damping present.

avoided, the inertia of the arm typically varies by less than an order of magnitude. Further, for our experiments the manipulator was close to a minimum inertia configuration. Therefore, higher inertia configurations would not invalidate the approximation of $\alpha \rightarrow 1$, nor greatly change K' and C'.

5 Simulation

To validate the parametric values obtained through experimentation and the approximations previously outlined, the values where employed in a simulation of the original fourth order model represented by Equations (1). Figure 13 shows the time response of the measured force, position, and velocity. This compares favorably with the real data in Figure 8. The frequency of the simulation is 84 radians/second, compared with 90 radians/sec for the data.

The simulated force versus velocity loop is shown in Figure 14. This is compared to the real data in Figure 11. The slope of 64 $\mathrm{N \cdot s/m}$ is very close to the data value of 66 $\mathrm{N \cdot s/m}$. Notice too, that this graph exhibits a positive skew axis, further justifying the earlier explanation of this phenomenon in Section 3.

The simulated force versus position loop is shown in Figure 15. This is compared to the real data in Figure 10. Although the slope of the skew axis is smaller in the simulation by about 30%, this can be attributed to the model inaccuracies and experimental error. Since we have been mainly concerned with the order of magnitudes of the spring constants, this is a reasonably good result.

The slope of the force versus position curve is determined mainly by the value of k_3. To improve its slope, k_3 can be increased by 30% to 13000 N/m. Changing k_3 alters other parameters also. The new values of the altered parameters are: $m_A = 1.46\,\mathrm{kg}$, $m_B = 0.14\,\mathrm{kg}$, $c_2 = 3651\,\mathrm{N \cdot s/m}$, and $c_3 = 26.3\,\mathrm{N \cdot s/m}$. The use of these parameters does not greatly alter the appearance of the previous simulation results, except making the slope of the $f(x)$ loop about the same as the experimental data [10].

6 The Resultant Model

The purpose of this analysis has been to obtain reasonable estimates of the system parameters. These values provide a plant model for developing and evaluating force control strategies. For these purposes, even order of magnitude approximations will prove to be acceptable. The correspondence between experimentation and simulation indicated that the developed fourth order model is accurate and useful.

This fourth order model has been used as the plant to correctly predict the behavior of a spectrum of force control strategies [11]. However, for that type of analysis it is more useful to use the pole/zero representation of the plant. The locations of the poles and zeros for this plant are shown in Figure 16. Figure 17 shows this same plot, but ignores the leftmost, insignificant pole on the real axis at -28000. The complex pole/zero pairs are due mainly to the environment. The other pole pair is due mainly to the sensor dynamics. It can be seen that the sensor poles are fairly far removed from the environmental ones, and are located farther into the left half plane. Usually, the leftmost sensor pole can be ignored.

It is important to note that the derived model parameters make the fourth order system extremely different than the one presented in [3]. In that discussion, based on theoretical analysis only, it was assumed that two (complex conjugate, sensor) poles are to the right of two (environmental) pole/zero pairs. As has been shown from experimental data, the sensor poles are

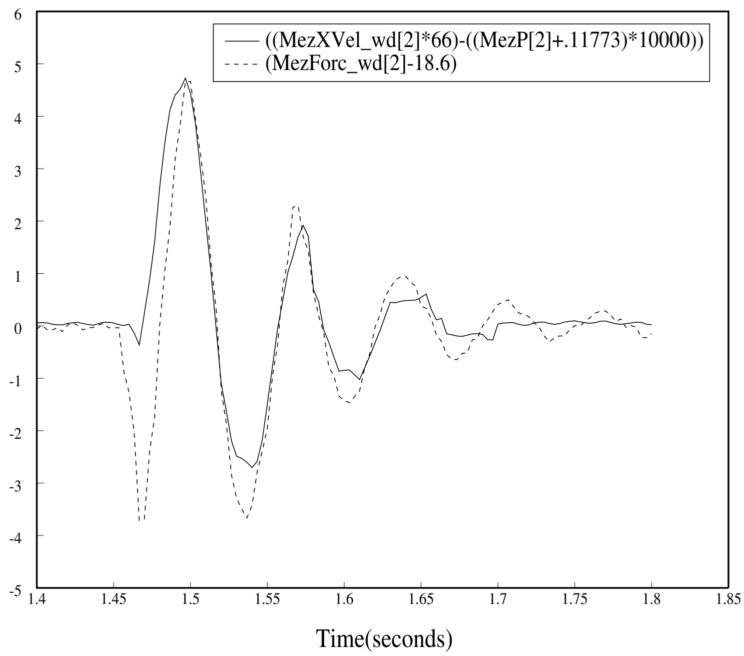

Figure 12: The addition of the measured position and velocity, multiplied by the determined constants, yields a close match to the measured force.

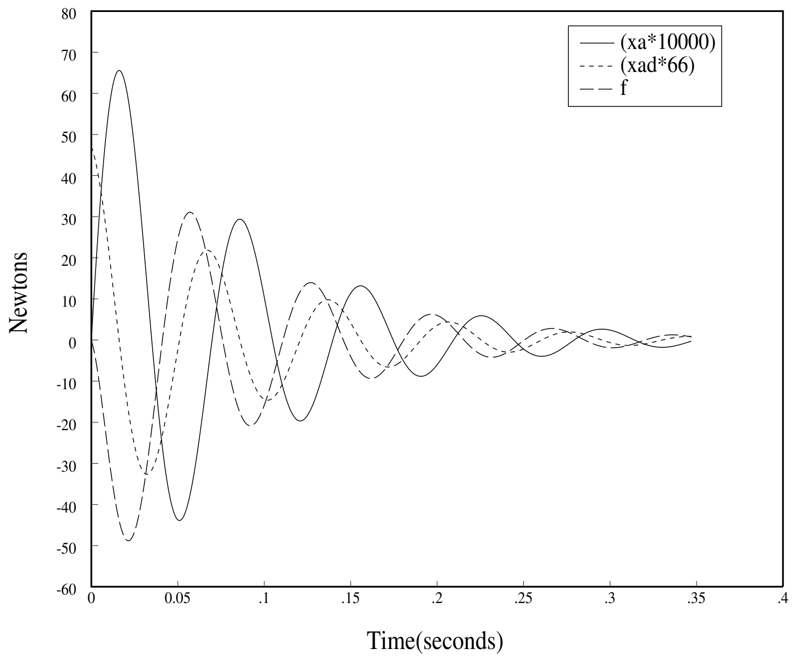

Figure 13: Simulated time response of position (solid), velocity (short dash), and force (long dash), using the estimated parameter values.

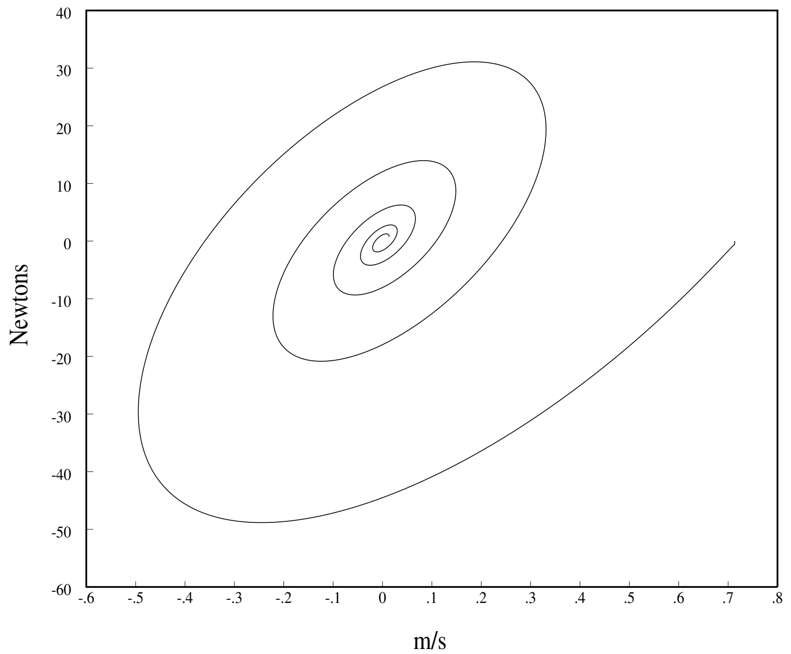

Figure 14: Simulation result of force versus velocity using estimated parameters.

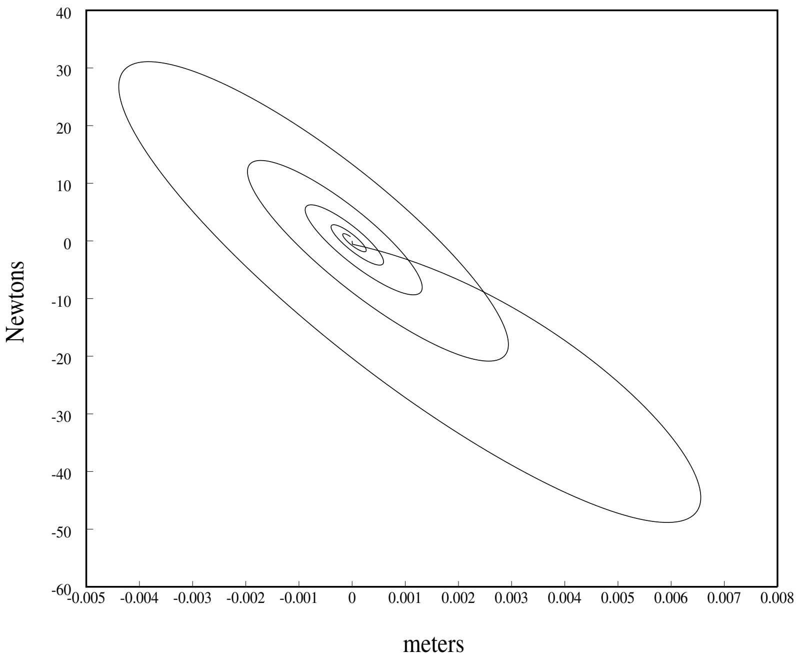

Figure 15: Simulation result of force versus position using estimated parameters.

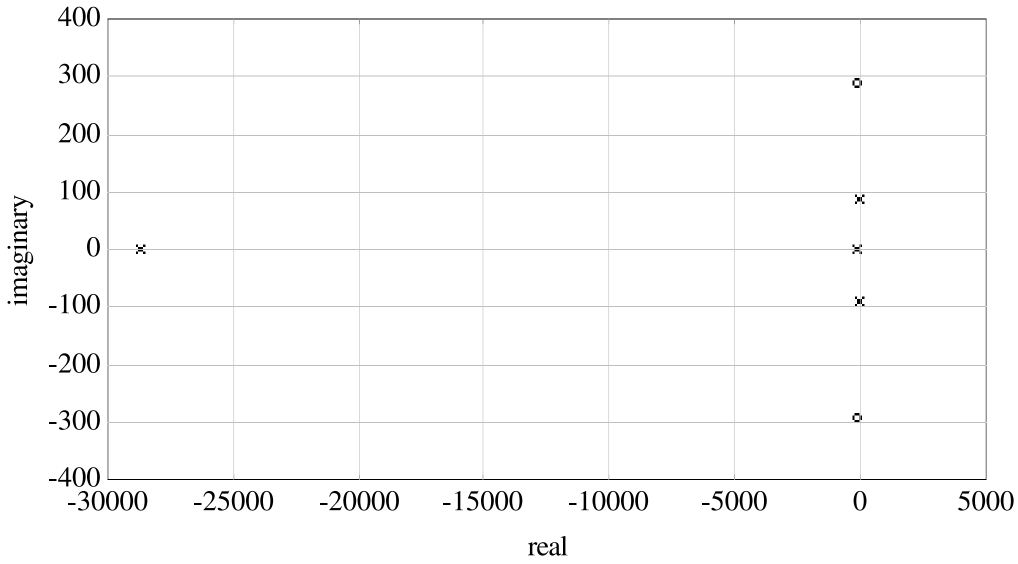

Figure 16: The poles and zeros of the fourth order system.

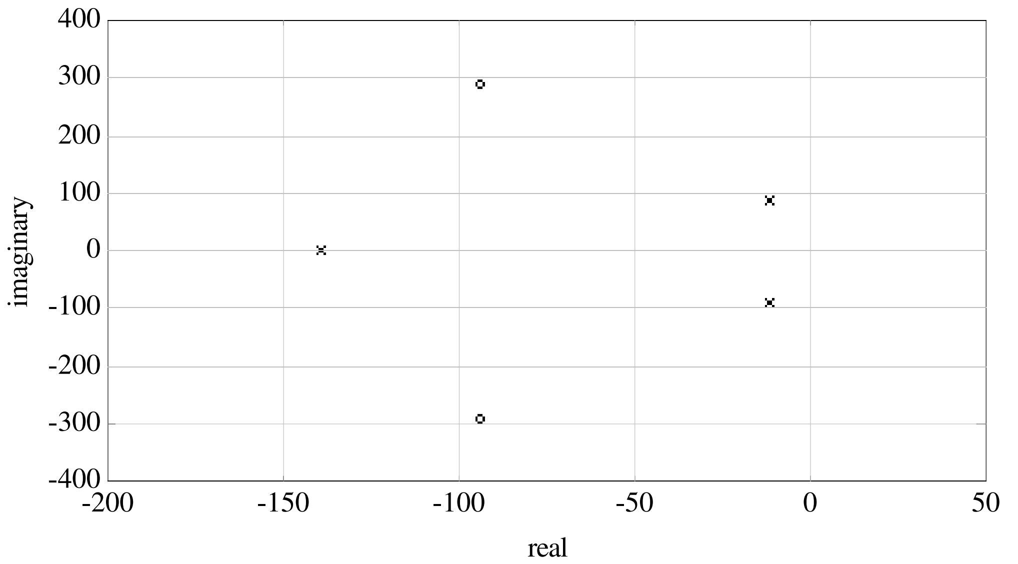

Figure 17: A pole/zero plot of the modelled system showing all but one pole which is on the real axis at approximately -28000.

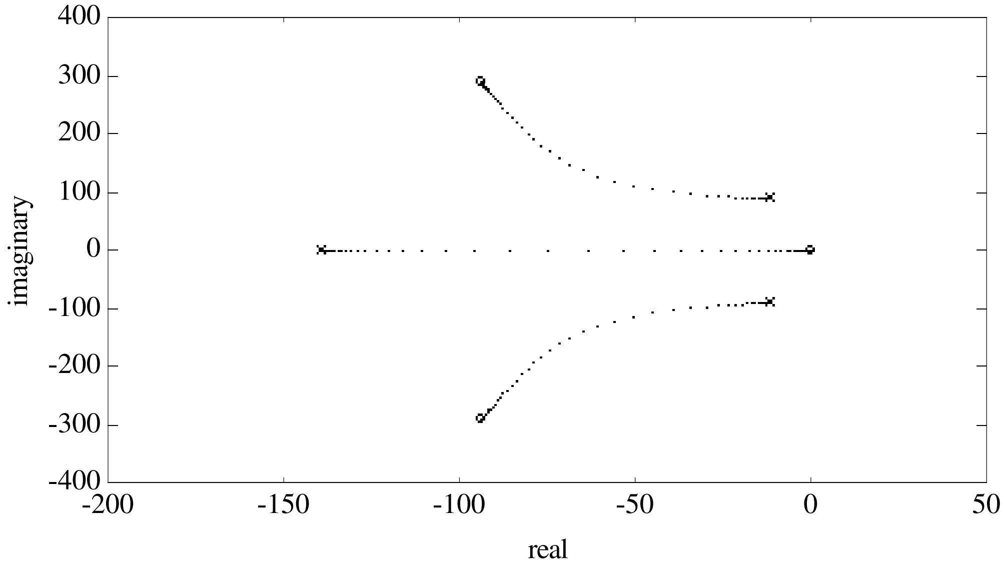

Figure 18: Root locus for the fourth order model under derivative gain explicit force control.

to the left and are real, for a very common environment. This difference in the arm / sensor / environment model results in erroneous predictions about the stability properties of common force control schemes [11]. For instance, integral gain control has been predicted to be a poor controller, while proportional gain control has been predicted to be always stable [3].

A more valid analysis of force control schemes can be obtained from using the experimentally obtained model parameters. Figures 18-23 show the root loci and Bode magnitude plots for proportional-derivative, proportional, and integral gain force controllers acting on the arm / sensor / environment plant. The PD controller analyzed in Figure 18 appears best since it keeps the poles in the left half plane. However, Figure 19 shows that it acts as a band-pass filter for the resonance frequencies of they system. This fact, and its amplification of noise, make it unstable in practice (without the addition of passive compliance) [11]. Alternatively, the proportional and integral controllers of Figures 20-23 have about the same pole structure near the origin, with the exception of the integral controller pole on the real axis. While both controllers can make the system unstable, the integrator pole provides valuable low-pass filtering as shown in Figure 23, and eliminates steady state error at lower gains.

Figures 24 and 25 show the best responses obtained for the proportional and integral gain controllers. Contrary to the previous predictions, but consistent with the predictions based on our experimentally derived model, the integral controller is superior. Further, experimentation showed that the proportional controller could easily be made unstable [13], directly contradicting previous predictions.

These results indicate the need for experimentally derived parameters, and validate the fourth order model of the system. The results also validate the model parameters obtained, as well as the method used to obtain them. However, it is important to note that it may not be necessary to employ this same method to analyze all arm / sensor / environment systems. Instead, a fourth order system assumption may be made in an adaptive scheme and real-time parameter identification may be possible. The analysis presented, however, has the benefit of giving physical insight into the derived model and its assigned parameters.

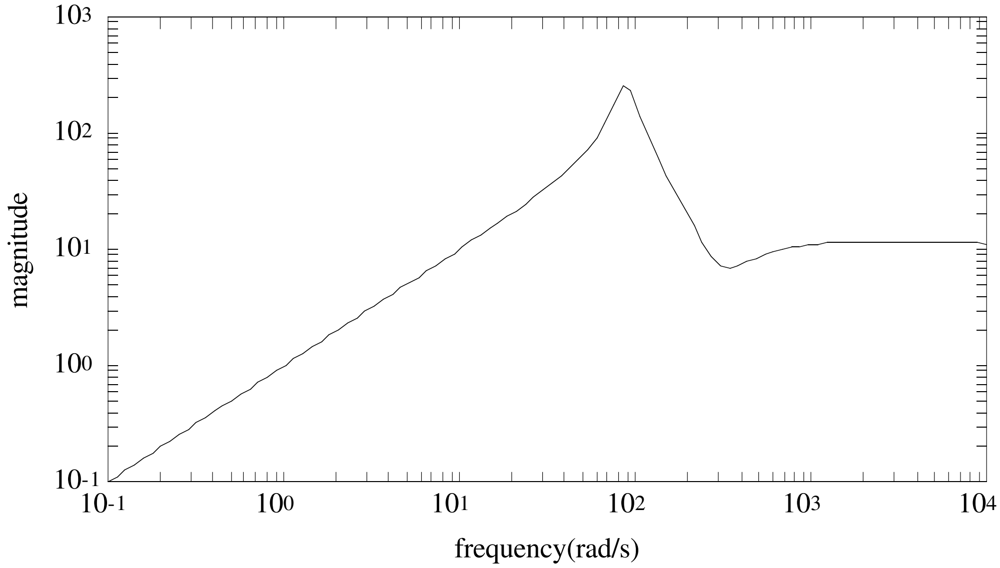

Figure 19: Bode plot for the fourth order system under derivative gain explicit force control. The resonance peak corresponds to the natural frequency of the environment. Thus, this controller acts as a band pass filter for the resonant frequency of the system.

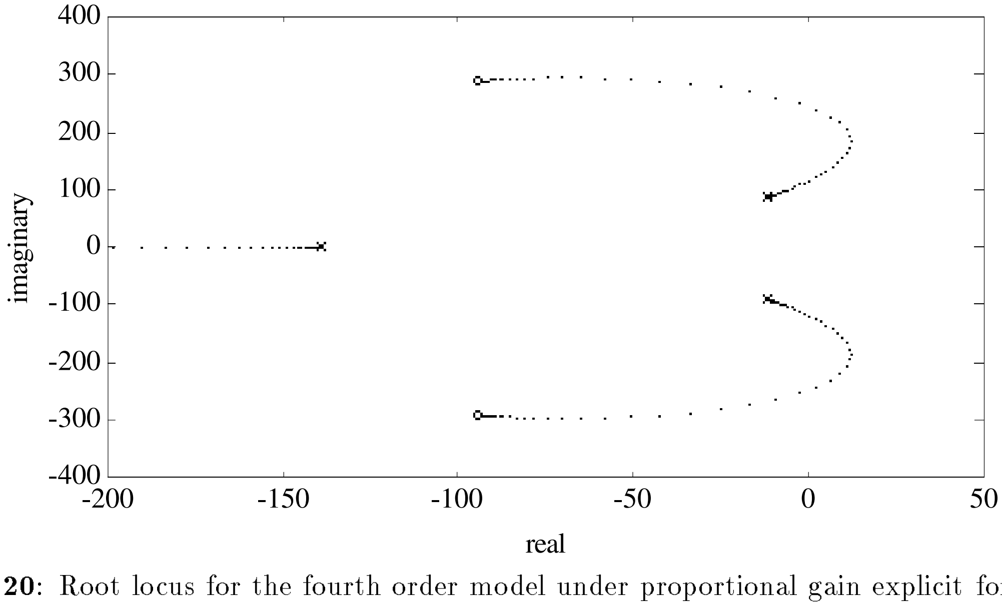

Figure 20: Root locus for the fourth order model under proportional gain explicit force control. The locus first crosses the imaginary axis for $K_{fp} \approx 1.2$.

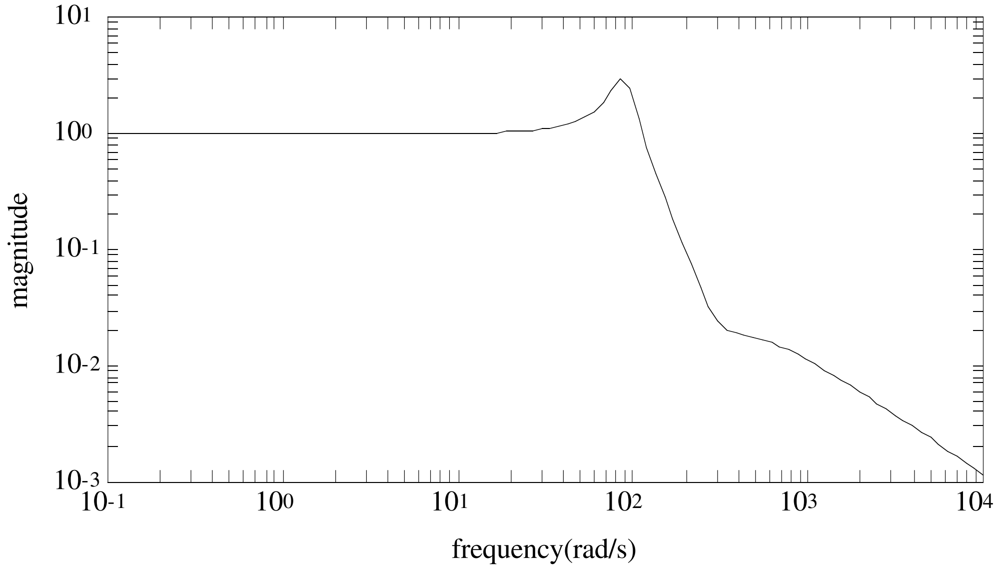

Figure 21: Bode plot for the fourth order system under proportional gain explicit force control. The resonance peak occurs near the natural frequency of the environment. The gain margin is 1.2 at $\omega = 118$ rad/s, which corresponds to the root locus crossing to the right half plane in Figure 20.

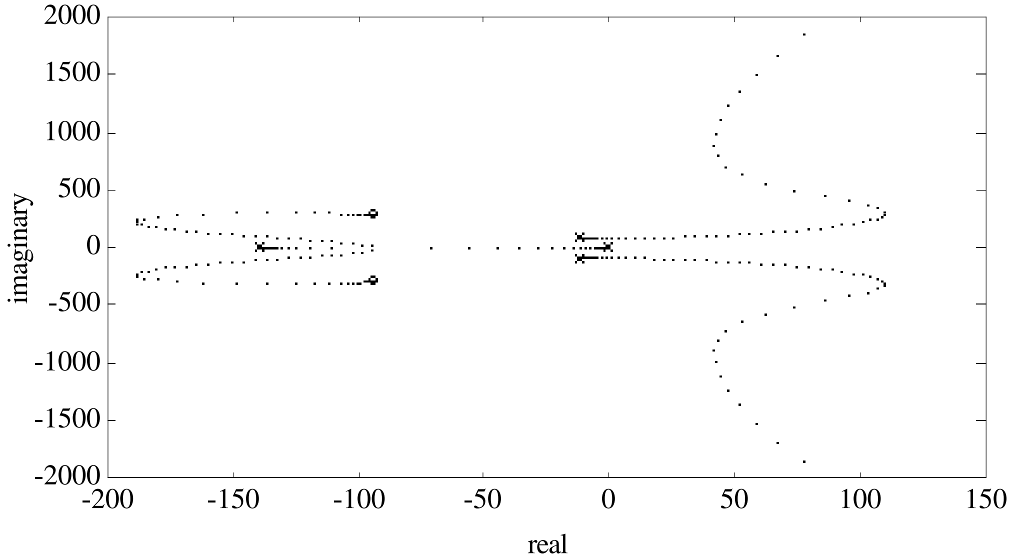

Figure 22: Root locus for the fourth order model under integral gain explicit force control.

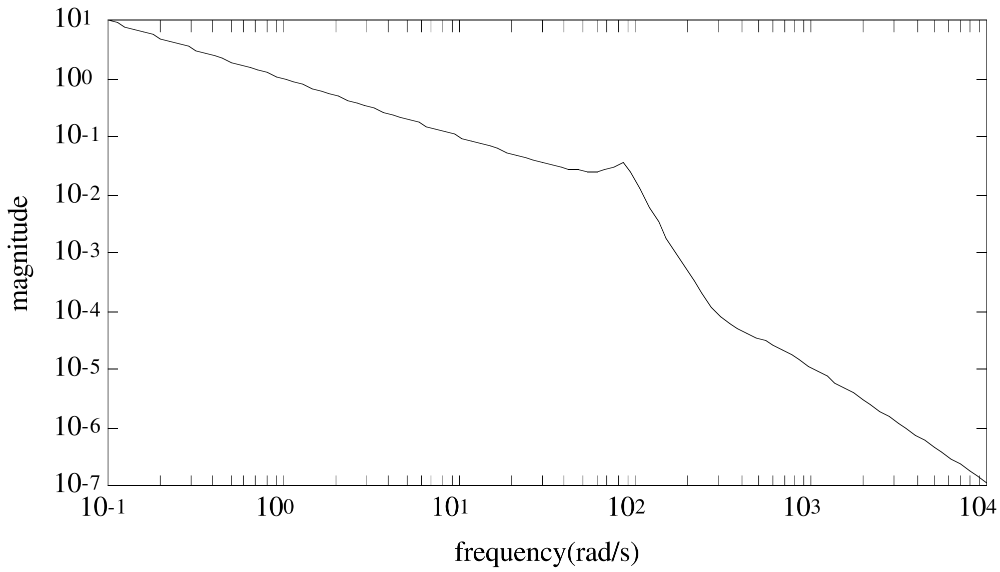

Figure 23: Bode plot for the fourth order system under integral gain explicit force control. The resonance peak corresponds to the natural frequency of the environment, but remains under a magnitude of one for gains of ~ 10. The gain margin is 28 at $\omega = 85$ rad/s, which corresponds to the root locus crossing to the right half plane in Figure 22.

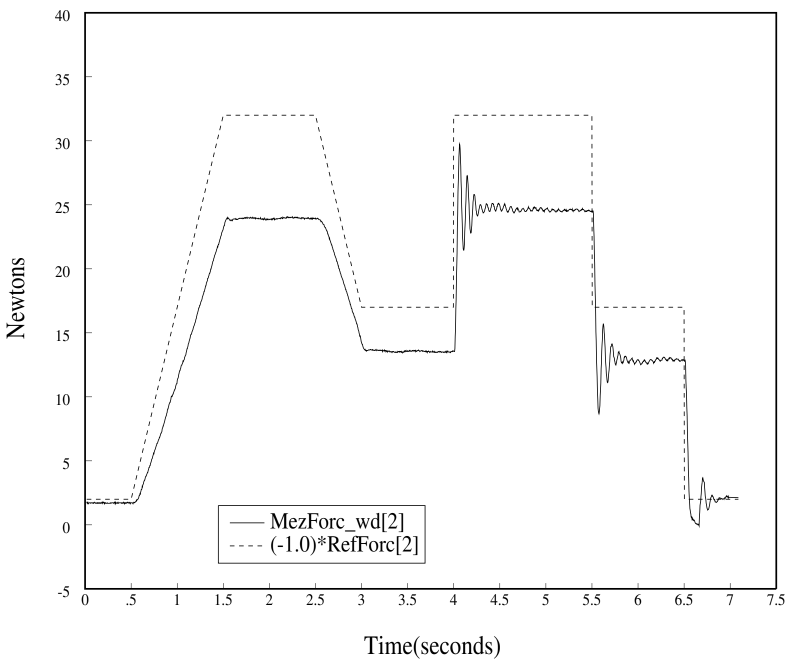

Figure 24: Experimental data of proportional gain explicit force control with feedforward and $K_{fp} = 0.5$.

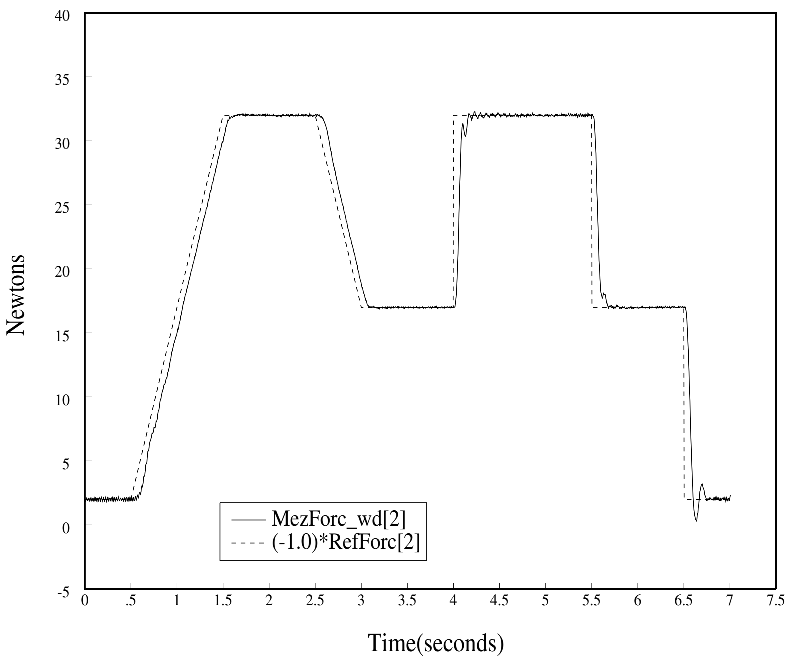

Figure 25: Experimental data of integral gain explicit force control with feedforward and $K_{fi} = 22.5$.

7 Conclusion

This paper has presented an analysis of an arm / sensor / environment model for force control of a robot manipulator in contact with its environment. First, a fourth order model was presented and vibration analysis of it was performed for both undamped and underdamped cases. This analysis described the oscillation modes of the system and predicted the form of the curves for force versus position and velocity. Experimental measurement of the real arm / sensor / environment system confirmed this predicted behavior. Further, quantitative analysis and judicious approximations made it possible to extract values for all system parameters. A simulation of the system using the extracted parameters matched the real system response, and confirmed the correctness of the values. Analysis of force controllers with this plant provided new predictions about the efficacy of each. Finally, some experimental results were provided, which matched the analysis, and thereby validated the plant model.

This research was valuable for three major reasons. First, real parameter values for the fourth order model were determined. Second, the match of the simulation with the real system response confirms the correctness of using the fourth order model, as well as the extracted parameter values. Third, the model has been used to analyze the efficacy and stability of many proposed force control strategies, and to understand the experimental results of tests of them [11, 12].

8 Acknowledgements

This research was performed at Carnegie Mellon University and supported by an Air Force Graduate Laboratory Fellowship (for Richard Volpe), DARPA under contract DAAA-21-89C-0001, the Department of Electrical and Computer Engineering, and The Robotics Institute.

The writing and publication of this paper was supported by the above and the Jet Propulsion Laboratory, California Institute of Technology, under a contract with the National Aeronautics and Space Administration.

The views and conclusion contained in this document are those of the authors and should not be interpreted as representing the official policies, either expressed or implied, of the U.S. Air Force, DARPA, or the U.S. Government. Reference herein to any specific commercial product, process, or service by trade name, trademark, manufacturer, or otherwise, does not constitute or imply its endorsement by the United States Government or the Jet Propulsion Laboratory, California Institute of Technology.

References

[1] C. An and J. Hollerbach. Dynamic Stability Issues in Force Control of Manipulators. In *Proceedings of the IEEE Conference on Robotics and Automation*, pages 890–896, 1987.

[2] R. Anderson and M. Spong. Hybrid Impedance Control of Robotic Manipulators. In *Proceedings of the IEEE Conference on Robotics and Automation*, pages 1073–1080, 1987.

[3] S. Eppinger and W. Seering. On Dynamic Models of Robot Force Control. In *Proceedings of the IEEE Conference on Robotics and Automation*, pages 29–34, 1986.

[4] S. Eppinger and W. Seering. Understanding Bandwidth Limitations on Robot Force Control. In *Proceedings of the IEEE Conference on Robotics and Automation*, pages 904–909, Raleigh, N.C., 1987.

[5] M. Raibert and J. Craig. Hybrd Position/Force Control of Manipulators. *Journal of Dynamic Systems, Measurement, and Control*, 103(2):126–133, June 1981.

[6] J. K. Salisbury. Active Stiffness Control of a Manipulator in Cartesian Coordinates. In *IEEE Conference on Decision and Control*, pages 95–100, New Mexico, 1980.

[7] K. Symon. *Mechanics*. Addison-Wesley, Reading, Massachusetts, 1960. textbook.

[8] W. Thomson. *Theory of Vibration with Applications*. Prentice Hall, NJ, 1981.

[9] R. Volpe. *Real and Artificial Forces in the Control of Manipulators: Theory and Experiments*. PhD thesis, Carnegie Mellon University, Department of Physics, September 1990.

[10] R. Volpe and P. Khosla. Theoretical Analysis and Experimental Verification of a Manipulator / Sensor / Environment Model for Force Control. In *Proceedings of the IEEE International Conference on Systems, Man, and Cybernetics*, Los Angeles, November 1990.

[11] R. Volpe and P. Khosla. A Theoretical and Experimental Investigation of Explicit Force Control Strategies for Manipulators. *IEEE Transactions on Automatic Control*, 38(11), November 1993.

[12] R. Volpe and P. Khosla. A Theoretical and Experimental Investigation of Impact Control for Manipulators. *International Journal of Robotics Research*, 12(4):351–365, August 1993.

[13] R. Volpe and P. Khosla. The Equivalence of Second Order Impedance Control and Proportional Gain Explicit Force Control: Theory and Experiments. In R. Chatila and G. Hirzinger, editors, *Experimental Robotics II*, pages 3–24, London, 1993. Springer-Verlag.

[14] R. Volpe and P. Khosla. Computational Considerations in the Implementation of Force Control Strategies. In *Journal of Intelligent and Robotic Systems: Theory and Applications. Special Issue on Computational Aspects of Robot Kinematics, Dynamics, and Control*, (accepted for publication in 1994).

[15] D. Whitney. Historical Perspective and State of the Art in Robot Force Control. In *Proceedings of the IEEE Conference on Robotics and Automation*, pages 262–268, 1985.

[16] K. Youcef-Toumi. Force Control of Direct-Drive Manipulators For Surface Following. In *Proceedings of the IEEE Conference on Robotics and Automation*, pages 2055–2060, 1987.